Kinetic Studies for Photocatalytic Degradation of Eosin B on a Thin Film of Titanium Dioxide

Shuhua Zhou and Ajay K. Ray*

Department of Chemical and Environmental Engineering, National University of Singapore, 10 Kent Ridge Crescent, Singapore 119260, Singapore

A semiconductor photocatalytic process has been studied extensively in recent years because of its intriguing advantages in environmental remediation. In this study, a two-phase swirl-flow monolithic-type reactor is used to study the kinetics of photocatalytic degradation of Eosin B for two different operating configurations: substrate-to-catalyst and liquid-to-catalyst illumination modes. True kinetic rate constants were determined as a function of the light intensity and catalyst layer thickness after correcting for mass-transfer limitation. In addition, the effects of several other parameters such as pH, dissolved oxygen, and temperature were examined. This new reactor appears to be an attractive choice for kinetic studies of heterogeneous photocatalysis.

Introduction

Heterogeneous photocatalysis has received considerable attention in recent years as a viable treatment technology for handling industrial effluents and contaminated drinking water. This is evident from the numerous review papers that have been devoted to this field.[1−13] The process couples low-energy ultraviolet light with semiconductors acting as photocatalysts. In this process, electron−hole pairs that are generated by the band-gap excitation carry out in situ degradation of toxic pollutants. The holes act as powerful oxidants to oxidize toxic organic compounds, while electrons can reduce toxic metal ions to metals, which can subsequently be recovered by solvent extraction.[14] Photocatalytic degradation offers certain advantages over the traditional water treatment methods. Complete destruction of most contaminants is possible without the need of additional oxidizing chemicals such as hydrogen peroxide or ozone. Degussa P25 TiO_2 is widely used as the photocatalyst, which requires UV-A light (λ < 380 nm) of intensity 1−5 W/m^2 for photoexcitation. The catalyst is cheap and can also be activated with sunlight.[11]

TiO_2 catalyst has been used in two forms: freely suspended in an aqueous solution and immobilized onto a rigid inert surface. In the former case, a high ratio of illuminated catalyst surface area to the effective reactor volume can be achieved for a small, well-designed photocatalytic reactor,[15] and almost no mass-transfer limitation exists because the diffusional distance is very small, resulting from the use of ultrafine (<30 nm) catalyst particles.[16] In large-scale applications, however, the catalyst particles must be filtered prior to the discharge of the treated water, even though TiO_2 is harmless to the environment. Hence, a liquid−solid separator must follow the slurry reactor. The installation and operation of such a separator will raise the cost of the overall process because the separation of the ultrafine catalyst particles is a slow and expensive process. Besides, the penetration depth of the UV light is limited because of the strong absorption by TiO_2 and dissolved organic species, particularly for dyes. All of these disadvantages render the scale-up of a slurry reactor very difficult.[17]

The preceding problem can be eliminated by immobilizing the TiO_2 catalyst over suitable supports.[18−21] The design and development of an immobilized thin catalyst film makes commercial-scale applications of TiO_2-based photocatalytic processes for water treatment possible.[22−24] The designs are more likely to be useful in commercial applications because they provide at least three important advantages. First, they eliminate the need for the separation of the catalyst particles from the treated liquid and enable the contaminated water to be treated continuously. Second, the catalyst film is porous and can therefore provide a large surface area for the degradation of contaminant molecules. Third, when a conductive material is used as the support, the catalyst film can be connected to an external potential to remove excited electrons to reduce electron−hole recombination, thereby significantly improving the process efficiency.[25] However, immobilization of TiO_2 on supports also creates its own problems.[26] There are at least two obvious problems arising from this arrangement: the accessibility of the catalytic surface to the photons and the reactants and a significant influence of the external mass transfer particularly at low fluid flow rate, because of the increasing diffusional length of the reactant from bulk solution to the catalyst surface. On the other hand, with an increase of the catalyst film thickness, the internal mass transfer may play a dominant role by limiting the utilization of the catalyst near the support surface. All of these usually lead to a lower overall degradation rate when the catalyst is immobilized compared with the suspended system.[18] Surprisingly, there are very few investigations[15,27,28] that offer a rational approach to study the influence of mass transfer in immobilized catalyst films, although studies in the photocatalytic field have reached the preindustry stage.

In this study, a novel semibatch swirl-flow monolithic-type reactor is used to study the kinetics of photocatalytic reactions. Monoliths are unique catalyst supports that provide a high surface-to-volume ratio and allow high flow rates with low pressure drop. The catalyst was immobilized for continuous use and to eliminate the

* To whom correspondence should be addressed. Fax: +65 6779 1936. E-mail: cheakr@nus.edu.sg.

10.1021/ie030366v CCC: $25.00
Published on Web 10/24/2003

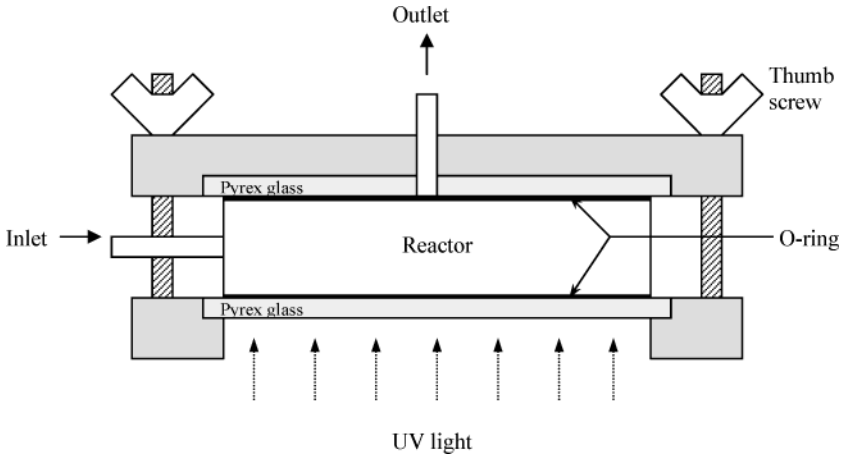

Figure 1. Schematic drawing of the kinetic reactor.

need of separation for postprocess treatment. Experiments are performed to determine the various rate constants. Experiments are also conducted to study the effect of light intensity and catalyst layer thickness on the reaction rate constants for two different operating modes, viz., when light falls directly on the catalyst [substrate−catalyst (SC) illumination] film and when light has to travel through the absorbing heterogeneous medium to activate the catalyst [liquid−catalyst (LC) illumination]. As is evident for most fixed-bed catalyst systems, mass-transfer limitations do exist. These are measured, and the results are corrected to obtain pure kinetic data. Fundamental experimental macrokinetic data on photocatalytic oxidation of Eosin B are investigated under conditions that are relevant for evaluation of the design of other reactors.

Experimental Details

Materials. Eosin B ($C_{20}H_6Br_2N_2Na_2O_9$, acid red 91, CI 45400, MW 624.1), a xanthene dye widely used as a biological stain, was provided by Sigma Co. Eosin B is widely used to estimate a wide range of proteins because in acidic solution Eosin B binds to proteins and absorption of the protein−dye complex around 536−544 nm is proportional to the concentration of the proteins. The stain is harmful if swallowed, inhaled, or absorbed through skin. Some researchers have tried to remove it by adsorption, but no one has attempted for complete degradation. This is an excellent model component for the characterization of a photocatalytic reactor, and the dye is reactive only in the presence of both TiO_2 and UV light and is biologically not degradable.

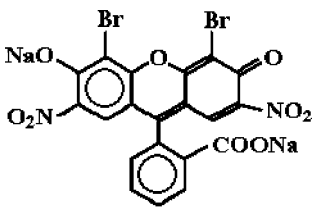

Degussa P25 catalyst provided by Degussa Co. (Germany) was used throughout this work without further modification. Its main physical data are as follows: Brunauer−Emmett−Teller surface area 55 ± 15 m^2/g, average primary particle size around 30 nm, purity above 97%, and anatase-to-rutile ratio 80:20. Nitric acid (65 wt %) and sodium hydroxide (98%) are from Baker

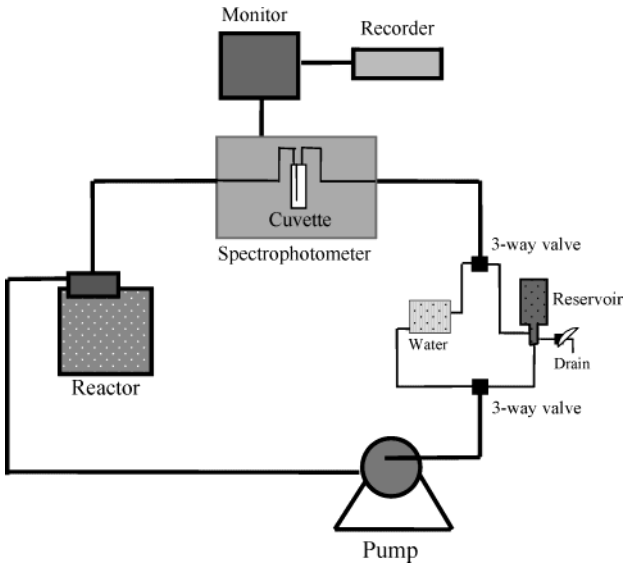

Figure 2. Flow diagram of the experimental setup.

Chemicals. All chemicals were used as received. Water used in this work was always from a Milli-Q plus 185 ultrapure water system.

Experimental Setup. The reactor consists of two circular glass plates each of diameter 0.05 m that are placed between soft padding housed within stainless steel and aluminum casing separated by 0.01 m (Figure 1). The catalyst was deposited either on the top of the bottom plate or on the bottom of the top plate. The aqueous solution was introduced tangentially into the reactor by a peristaltic pump from a beaker with a water jacket and exited from the center of the top plate (Figure 2). The exit tubing was also connected to that beaker. The tangential introduction of liquid created a swirl flow, thereby minimizing mass transfer of pollutants to the catalyst surface. The flow pattern inside the reactor of the same dimension as that used in this study was simulated using a commercial CFD software package, Fluent. In Figure 3, the particle trajectory is shown for an inlet flow rate of 5.0×10^{-5} m^3/s. The figure shows that tangential introduction of fluid indeed creates swirl flow inside the reactor. The lamp (Philips HPR 125 W high-pressure mercury vapor) was placed 0.01 m underneath the bottom glass plate on a holder that could be moved to create a different angle of incidence of light on the catalyst plate. The lamp and reactor were placed inside a wooden box painted black so that no stray light

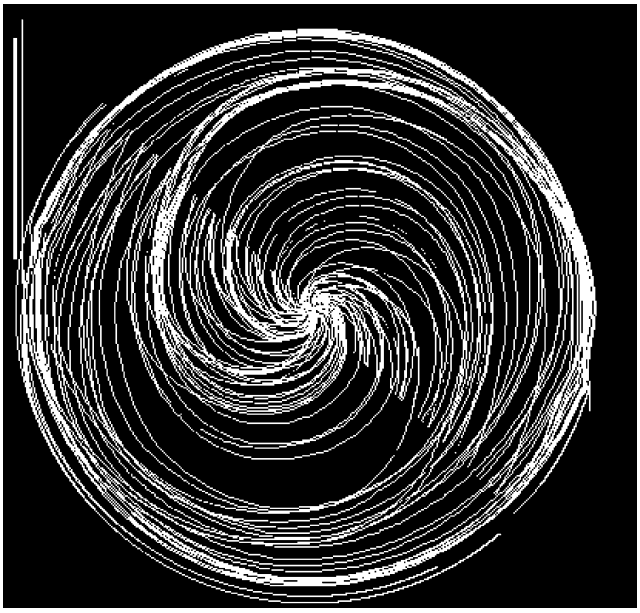

Figure 3. Flow pattern inside the reactor.

can enter into the reactor. The lamp was constantly cooled by a fan to keep the temperature down and protect the lamp from overheating. The lamp has a spectral energy distribution with a sharp peak at $\lambda =$ 365.5 nm of 2.1 W, and thereby the incident light intensity was 213 W/m^2. Provision was made for placement of several metal screens of different mesh sizes between the lamp and the bottom glass plate to obtain variation in light intensity. The light intensity was measured using a radiometer (Cole-Parmer 9811-58). Changes in the Eosin B dye concentration were measured by a Shimadzu UV 1601 PC spectrophotometer. A Shimadzu TOC-5000A analyzer with an ASI-5000 autosampler was used to analyze the total organic carbon in the samples. A Cyberscan 2000 pH meter was used to measure the pH value of the solution. The effective surface areas of the catalyst that is illuminated and the volume of the reactor are 1.963×10^{-3} m^2 and 1.963×10^{-5} m^3, respectively. For the reactor, κ, defined as the ratio of illuminated surface area of catalyst that is in contact with reaction liquid, equals 100 m^2/m^3.

Immobilization of the Catalyst. Pyrex (the surface was roughened by sand blasting for improved catalyst fixation) was chosen as the support material because it is transparent to UV radiation down to a wavelength of about 300 nm. Moreover, it would cutoff any light below 300 nm to avoid direct photolysis taking place. The glass surface was carefully degreased, cleaned with a 5% HNO_3 solution overnight, washed with water, and then dried at 393 K. A 10% aqueous suspension of the catalyst was prepared with water out of a Millipore Milli-Q water purification system. The suspension was mixed in an ultrasonic cleaner (Branson 2200) bath for 1800 s to obtain a milky suspension that remained stable for weeks. The substrate was then coated with catalyst by inserting it into the suspension and pulling it out slowly by a dip-coating technique.[15] The catalyst coating was dried at 393 K for 1800 s and then calcined in a furnace (Heraeus UT 6060) in a vertical position by raising the temperature gradually at a rate of 0.15 K/s (to avoid cracking of the film) to a final firing temperature of 573 K and holding it there for 10 800 s. Then, the glass plate was cooled to room temperature using the same ramping rate. It is necessary to heat

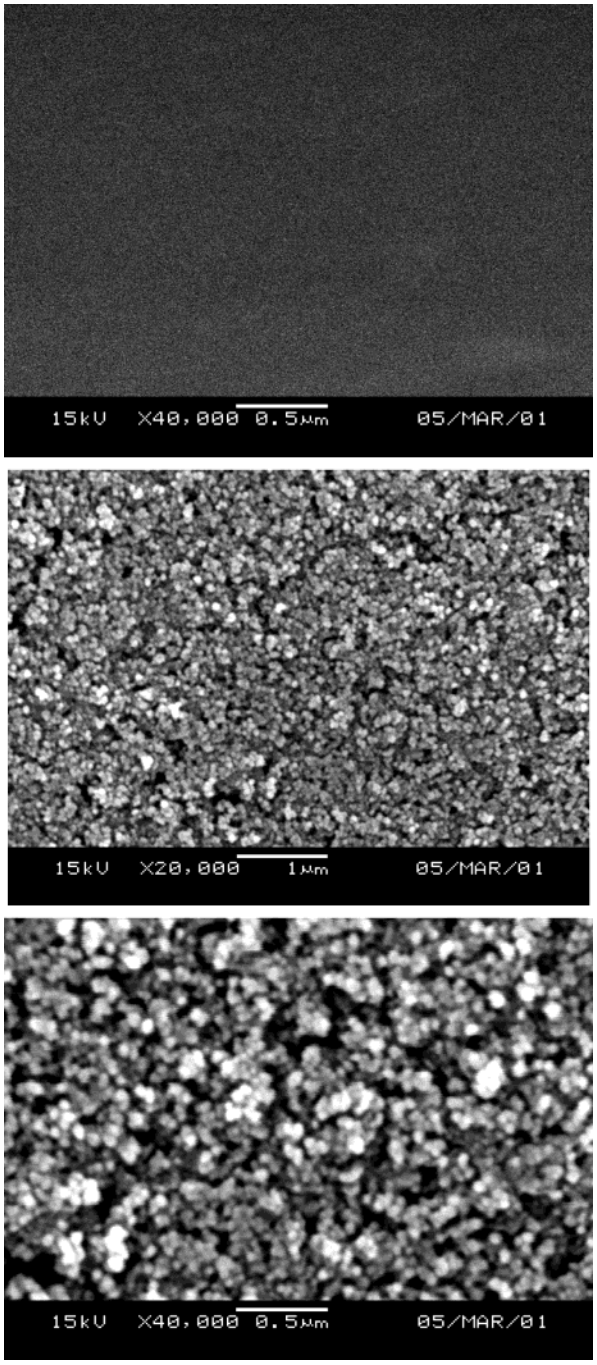

Figure 4. Scanning electron micrographs showing TiO_2 films deposited on Pyrex glass: (a) sand-blasted surface with no catalyst; (b and c) sand-balsted surface with catalyst ($w = 1.2 \times 10^{-2}$ kg/m^2).

and cool the glass plate gradually or the catalyst film may crack. The above procedures could be repeated a few times depending on the desired catalyst loading (thickness). The calcination temperature has a significant effect on the catalyst activity because it can affect the physical properties of the catalyst, such as porosity, surface area, crystal size, etc. Chen and Ray[27] have reported that the optimal calcination temperature is about 573 K. Finally, the catalyst film was brushed carefully and flushed with Millipore water to remove the loosely bound catalyst. The total amount of catalyst deposited per unit area was determined by weighing the glass plate before and after the deposition. Depending on the number of dippings, the amount of catalyst

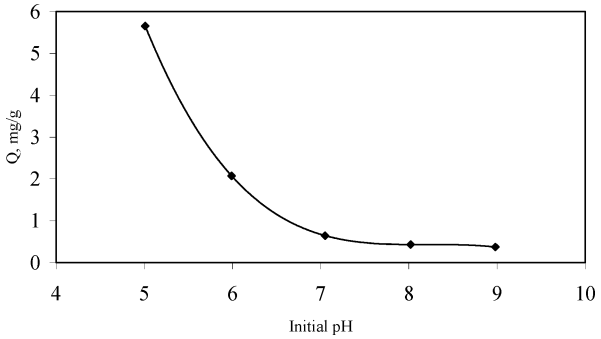

Figure 5. Effect of the initial pH on the adsorption of Eosin B on a TiO_2 catalyst surface. Experimental conditions: $C_0 = 16$ mmol/m^3, $Re = 141$, $V_L = 2.40$ m^3, $w = 5.2 \times 10^{-3}$ kg/m^2, $T = 303$ K, catalyst on the bottom plate.

obtained was between 0.003 and 0.02 kg/m^2. Figure 4 shows scanning electron micrograph pictures illustrating the surface morphology of a roughened (sand-blasted) glass plate with no catalyst and TiO_2 films containing 0.012 kg/m^2 of catalyst.

Experimental Procedures. Before a catalyst plate was placed inside the reactor, the light intensity on the top of the bare glass plate was measured with a digital radiometer. At the start of every experiment, the reactor was filled with Milli-Q water and rinsed for several times before zero-setting the analytical instrument. The reactor and connecting lines were then filled with the Eosin B solution, and it was ensured that no air bubbles remained in the system. The change in the concentration was continuously analyzed and recorded. Before the light is turned on, it is necessary to circulate this solution for about 1800 s to ensure that the adsorption equilibrium of the pollutant on the TiO_2 surface and oxygen presaturation of the solution has been reached. Oxygen was introduced to the solution continuously to keep the concentration of oxygen in excess of the stoichiometric requirement throughout the reaction. Later, some experiments were conducted to study the effect of oxygen. The flow rate of oxygen was measured by a gas flowmeter (Tokyo Keiso, Japan, model P-200-UO). At the end of the experiment, the entire system was rinsed with Milli-Q water and the catalyst plate was removed, dried, and weighed again to determine any loss of catalyst during experimentation. The total volume of the solution was always 2.40×10^{-4} m^3.

Results and Discussion

Before the start of the photocatalytic reactions, experiments were conducted to investigate whether there is any direct photolysis (in the presence of light but in the absence of any catalyst). It was observed that no direct photolysis takes place for Eosin B. When experiments were conducted in the presence of catalyst but in the absence of light (dark reaction), a small decrease in the concentration of Eosin B was observed because of adsorption of the model compound onto the catalyst surface, which reached an equilibrium value within 900 s. Hence, before the light was turned on, it was always ensured that adsorption equilibrium was reached. Therefore, degradation of Eosin B in the presence of light and catalyst observed is entirely due to photocatalysis.

Effect of the Initial pH. The pH of the reaction medium has a significant effect on the surface properties of the TiO_2 catalyst, which include the surface charge of the particles, the size of the aggregation of the catalyst particles it forms, and the band edge position of TiO_2. Because a photocatalytic degradation reaction takes place on the surface of the catalyst, the photocatalytic reaction, in general, is pH-dependent although the rate varies by less than 1 order of magnitude between pH 2 and 12 (2, 6). The point of zero charge (pH_{zpc}) for Degussa P25 TiO_2 is at a pH equal to 7.2. The amount of positive charges on the TiO_2 surface decreases with increasing pH and reaches zero at pH_{zpc}. Therefore, pH significantly affects the adsorption−desorption properties of the model compounds on the

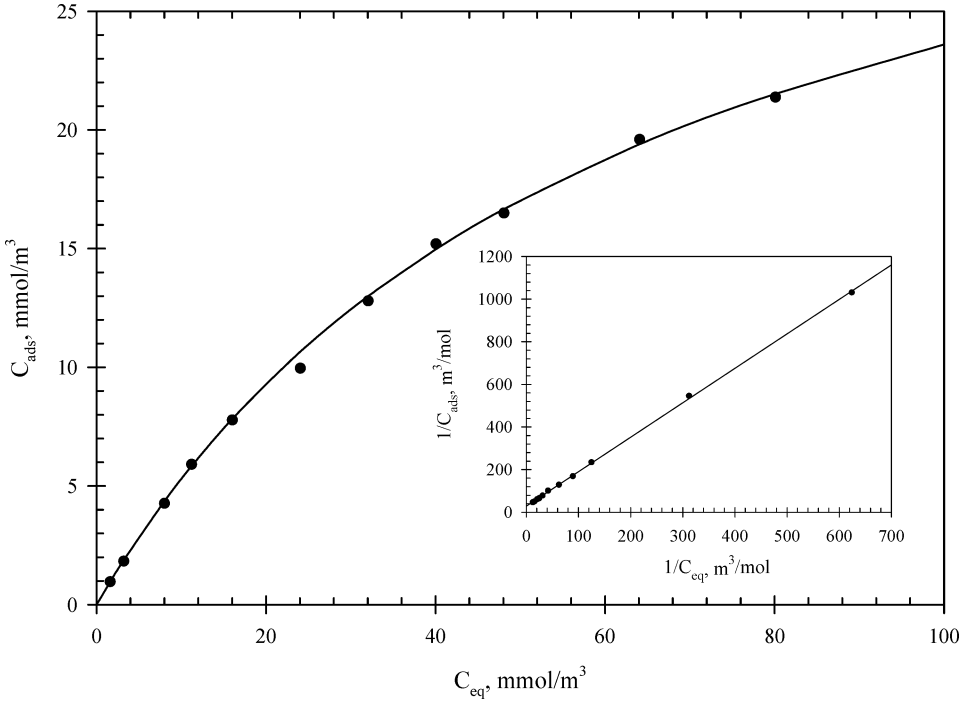

Figure 6. Calculation of the adsorption rate constant from a dark reaction. Experimental conditions: $Re = 141$, $V_L = 2.4 \times 10^{-4}$ m^3, $w = 5.2 \times 10^{-3}$ kg/m^2, $T = 303$ K, catalyst on the bottom plate.

surface of the catalysts. The adsorption experiments of Eosin B on TiO_2 were conducted at different initial pH values (Figure 5). The figure clearly shows that adsorption of Eosin B decreases with increasing pH. The adsorption is particularly very low in alkaline conditions. This is expected because Eosin B in an aqueous solution ionizes and has a negative charge and, therefore, the adsorption amount decreases rapidly as the pH increases.

Most experiments were conducted starting with an initial pH of 5 but allowed to continue at natural pH to avoid any interference caused by the adsorption of buffer salts on the catalyst surface. In some cases (see later), 1 M nitric acid or sodium hydroxide was used to adjust the pH value of the solution to investigate the effect of pH on the reaction rate.

Dark Reaction: Determination of the Adsorption Equilibrium Constant. Adsorption equilibrium constants were determined from both dark reaction and photocatalytic reaction. The small rapid decrease in the Eosin B concentration in the absence of light (dark reaction) when a fresh catalyst plate was used can be attributed to the adsorption of Eosin B onto the catalyst. The concentration of Eosin B adsorbed on the surface was calculated from the difference between the initial and equilibrium (no more decrease with time) concentrations. When the results are plotted (Figure 6), they appeared to follow a Langmuir adsorption isotherm:

$$C_{ads} = \frac{NKC_{eq}}{1 + KC_{eq}} \tag{1}$$

where C_{ads} and C_{eq} are the concentration of Eosin B adsorbed and the equilibrium concentration of Eosin B used, respectively, and N and K are the saturation and adsorption equilibrium values, respectively. When the data were fitted with eq 1 or by a straight line in a $[1/C_{ads}]$ versus $[1/C_{eq}]$ plot, N and K were found to be 0.032 mol/m^3 and 16.1 m^3/mol, respectively.

Rate Expressions. Heterogeneous photocatalytic degradations often follow Langmuir−Hinshelwood kinetics. For our semibatch system, the intrinsic reaction rate, r_{rxn}, could be defined as

$$r_{rxn} = \left[\frac{V_L}{V_R}\right]\left[-\frac{dC_b}{dt}\right] = \frac{k_r K C_s}{1 + KC_s} \tag{2}$$

where V_L and V_R are the total volume of liquid treated (m^3) and volume of the reactor (m^3), respectively, dC_b/dt is the observed rate (mol/m^3/s), k_r and K are the reaction rate constant (mol/m^3/s) and (lumped) adsorption−desorption equilibrium constant (m^3/mol), respectively, and C_s is the concentration of the reactant at the catalyst surface (mol/m^3) in equilibrium with the actual surface concentration. It is to be noted that it is difficult to estimate for both slurry and immobilized catalyst systems the exact value for the active catalyst surface area participating in photocatalytic reactions. In the case of slurry systems, it is impossible to quantify the active surface area because of unreliable knowledge of the depth of light penetration, pattern of catalyst mixing, average catalyst particle size (and distribution) due to agglomeration, etc. It is also very difficult to determine the active surface area in fixed (immobilized) catalyst systems because the structure, morphology, porosity (interparticle pore distributions), and catalyst layer thickness vary. It is, therefore, impractical to compare the rates based on the active surface area for both the slurry and immobilized systems.

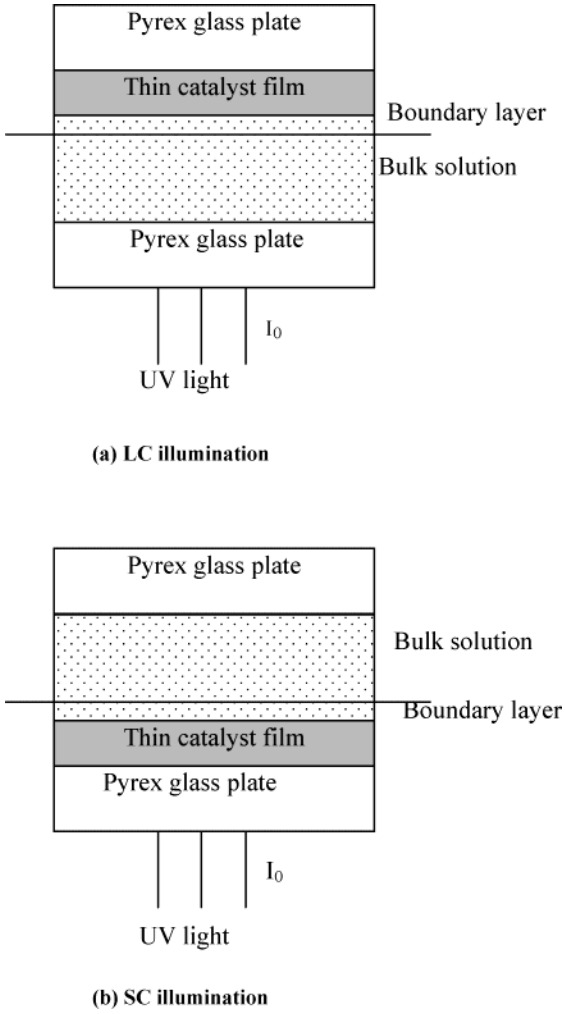

Figure 7. Schematic diagram to illustrate the representation of (a) LC illumination and (b) SC illumination.

Effect of the Catalyst Layer Thickness on the Degradation Rate: LC and SC Illumination. Experiments were conducted to study the photocatalytic degradation rate of Eosin B when the catalyst was coated either on the bottom plate or on the top plate. In the later case, the UV light will have to pass through the reaction medium before reaching the catalyst surface. Thus, the light intensity falling on the catalyst surface will be decreased considerably because of the light absorption by the reaction medium. These two cases are depicted as SC and LC illumination. The nomenclature used is to point out that the catalyst is activated from the substrate side (SC) or is activated from the liquid side (LC). The pollutant (contaminant) diffuses from the bulk solution through a boundary layer (liquid-film mass-transfer resistance) to reach the liquid−catalyst interface. Subsequently, the reactant diffuses through the catalyst layers (interparticle diffusion) to locate the active catalyst surface sites where they get adsorbed and react. It should be noted that Degussa P25 TiO_2 is a nonporous catalyst; thus, there is no intraparticle diffusion. At the same time, UV light must also reach the catalyst surface to activate the catalyst. It is worth noting that there is no boundary resistance for UV light penetration (transmission). Figure 7 is a schematic representation of LC and SC illumination.

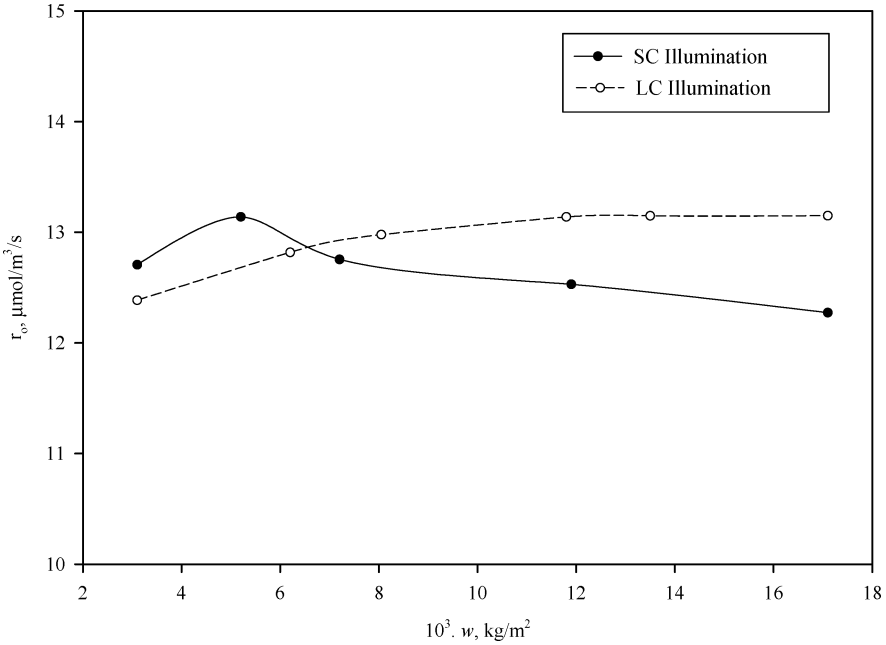

Figure 8. Effect of the catalyst layer thickness on the photocatalytic degradation rate of Eosin B. Experimental conditions: $C_0 = 16$ mmol/m^3, $Q = 5 \times 10^{-6}$ m^3/s, $I = 33$ W/m^2, $V_L = 2.4 \times 10^{-4}$ m^3, $T = 303$ K, $p_{O_2} = 60.8$ kPa, natural pH.

The catalyst layer thickness (amount of catalyst) is an important parameter in photocatalytic degradation. As in an aqueous suspension, there also exists an optimal catalyst dosage for a fixed catalyst system, particularly when the catalyst loading is increased. This is due to the increase of internal (interparticle) mass-transfer resistance, which will result in a decrease of the overall reaction rate. Ray and Beenackers[15] were the first to report some studies on the effect of the catalyst layer thickness on the photocatalytic degradation of SBB textile dye. Subsequently, Chen et al.[28] reported a detailed analysis of the effect of mass transfer and catalyst layer thickness on the photocatalytic degradation rate using benzoic acid as the model component. In this work, experiments were performed for photocatalytic degradation of Eosin B using different catalyst layer thicknesses for both SC and LC illumination configurations. The experimental results are shown in Figure 8 for both SC and LC illumination. Experimental results show that the photocatalytic rate goes through a maximum for SC illumination while it is constant for LC illumination when the catalyst film layer thickness is increased.

It is obvious that the observed reaction rate for SC illumination is greater than that for LC illumination when the film is thin. This is expected because, in the LC illumination case, the UV light has to pass through the reaction medium (solution) to reach the top glass plate where the catalyst is present. Hence, some photons are absorbed by the reaction medium, reducing the effective intensity of light. However, the most contrasting behavior observed between the SC and LC illumination is the existence of a unique optimal catalyst layer thickness for SC illumination. Figure 8 shows that for SC illumination the observed rate increases until a catalyst loading of 5.2×10^{-3} kg/m^2 is reached and the reaction rate decreases thereafter. However, for LC illumination, the reaction rate increases until a catalyst loading of 8.1×10^{-3} kg/m^2 is reached and remains almost constant subsequently instead of decreasing as in SC illumination. Therefore, there exists an optimal catalyst loading when catalyst is immobilized onto a substrate.

There are two likely loss mechanisms within the catalyst films due to an increase of the catalyst layer thickness that will restrict the presence of charge carriers at the interface. One is attenuation of light due to absorption by the catalyst, and the other is the increased probability of charge carrier recombination presumably due to the increased diffusional lengths through the grain boundaries and constrictions within the microporous film. Within the bulk of the catalyst film, the extinction of light follows the exponential decay.[28] Figure 8 indicates that the photocatalytic rate reaches a saturation value as the catalyst layer thickness increases. This can be understood if we look at the physical problem. When the catalyst film is thin, the absorption of light will not be strong enough because the wavelength of light ($\lambda = 0.365$ μm) is of the same order of magnitude as that of the film thickness and, consequently, the catalyst layer will not be active to its highest possible level. As the film thickness increases, at some point, light will be completely absorbed by the catalyst layer and the photocatalytic reaction rate will be at a maximum. With a further increase in the film thickness, the rate would remain constant because the diffusional length of the charge carrier to the catalyst−liquid interface will not change. However, when the light is introduced from the catalyst side (SC illumination), the state of affairs is slightly different. When the film is thin, the absorption of light is not strong enough and, consequently, the catalyst layer in contact with the liquid will not be active to its highest possible level. As the film thickness increases, at some point, the penetration depth of light will be such that most of the electrons and holes are generated relatively close to the solid−liquid interface. The photocatalytic reaction rate will be about maximum at this point. With a further increase in the film thickness (thicker film), the charge carriers are generated relatively far from the liquid−catalyst

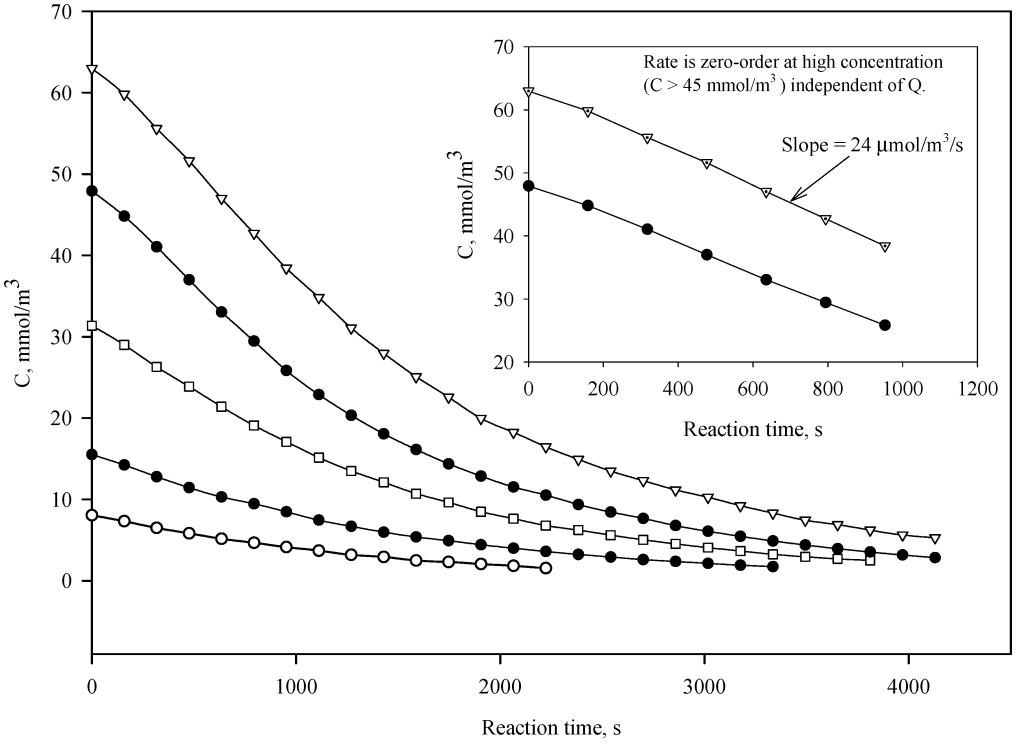

Figure 9. Photocatalytic degradation of Eosin B at different initial concentrations. Experimental conditions: SC illumination, $Q = 5.0 \times 10^{-6}$ m^3/s, $I = 33$ W/m^2, $w = 5.2 \times 10^{-3}$ kg/m^2, $V_L = 2.4 \times 10^{-4}$ m^3, $T = 303$ K, $p_{O_2} = 60.8$ kPa, natural pH.

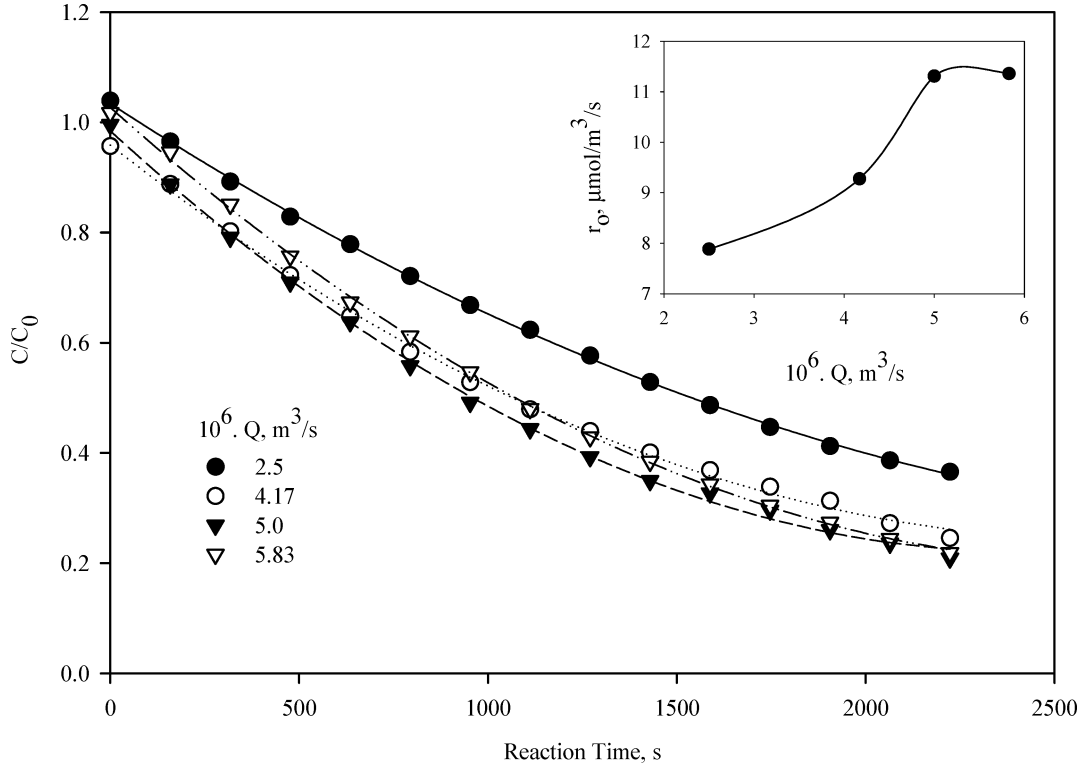

Figure 10. Effect of the circulation rate on the photocatalytic degradation rate of Eosin B. Experimental conditions: SC illumination, $C_0 = 16$ mmol/m^3, $I = 33$ W/m^2, $w = 5.2 \times 10^{-3}$ kg/m^2, $V_L = 2.4 \times 10^{-4}$ m^3, $T = 303$ K, $p_{O_2} = 60.8$ kPa, natural pH.

interface and, consequently, are more susceptible to recombination loss. For SC illumination, a further increase of the film thickness will lower the photocatalytic reaction rate. This is in contrast to LC illumination, where the rate remains constant.

Effect of the Initial Concentration: Determination of the Reaction Rate Constant. The initial concentration of the pollutant is always an important parameter in any process water treatment and, therefore, it is essential to examine the effect of the initial concentration. However, when the TiO_2 catalyst is coated on a support, it is expected that the mass-transfer limitation would play a significant role in photocatalytic reactions because of the increased diffusional length for diffusion of contaminants from the bulk solution to the catalyst surface. Therefore, to determine

the intrinsic kinetic rates, it is necessary to eliminate the effect of mass transfer.

The kinetic expression in eq 2 is of the Langmuir type, and it was found to be true when experiments were performed in slurry systems. Therefore, when the catalyst is immobilized, it would not be possible to determine the kinetic parameters without knowing the concentration of the pollutant on the surface of the catalyst (C_s). However, when the initial concentration of the pollutant is high ($KC_s \gg 1$), the Langmuir-type kinetic rate expression collapse to a zero-order rate expression and the overall rate would not depend on external mass transfer. Therefore, if the experiment is performed when the catalyst film is thin (negligible internal mass-transfer resistance) with a high starting concentration of Eosin B and if the concentration versus time plot shows a linear relationship, it would imply that the rate is zero-order. Figure 9 shows the plot of the concentration with time for five different initial concentration values of Eosin B. The figure also reveals that the $C-t$ plot follows a linear relationship when experiments were done at a high initial concentration ($C_0 \geq 0.045$ mol/m^3). The true kinetic rate (k_r) can be determined from the slope of the concentration versus time plot and is obtained as 24 μmol/m^3/s.

It should also be noted that when the initial concentration of the pollutant is very low ($KC_s \ll 1$), the kinetic rate expression given by eq 2 becomes a first-order rate expression. In this case, the overall rate would certainly depend on mass transfer. For evaluation of the true kinetic parameters, it is necessary to eliminate mass-transfer resistance. At steady state, the conversion rate follows:

$$r_0 = \left[\frac{V_L}{V_R}\right]\left[-\frac{dC_b}{dt}\right] = k_o C_b = k_{m,ext}\kappa(C_b - C_s) = \frac{k_r K C_s}{1 + KC_s} \quad (3)$$

where C_b and C_s are the concentrations in the bulk and close to the catalyst surface, respectively, in mol/m^3, k_o (s^{-1}) is the first-order observed rate constant, k_m (m/s) is the mass-transfer rate, and κ (m^{-1}) is the specific surface area ($\equiv A/V_R$). However, when $KC_s \ll 1$, eq 3 becomes

$$r_0 = k_{m,ext}\kappa(C_b - C_s) = k_r K C_s = k_r' C_s \quad (4)$$

where k_r' is the first-order reaction rate constant (s^{-1}).

From the above equation, we can solve for the unknown concentration C_s as

$$C_s = \left(\frac{k_{m,ext}\kappa}{k_{m,ext}\kappa + k'}\right)C_b \quad (5)$$

The above equation can be substituted in eq 4 to give

$$r_o = k_o C_b = \left(\frac{k_r' k_{m,ext}\kappa}{k_{m,ext}\kappa + k_r'}\right)C_b = \left(\frac{1}{\frac{1}{k_r'} + \frac{1}{k_{m,ext}\kappa}}\right)C_b \quad (6)$$

In other words, the various rates (observed, kinetic, and mass-transfer rates) are related as

$$\frac{1}{k_o} = \frac{1}{k_r'} + \frac{1}{k_{m,ext}\kappa} = \frac{1}{k_r K} + \frac{1}{k_{m,ext}\kappa} \quad (7)$$

In addition to external mass-transfer resistance, when a catalyst is immobilized on a surface, internal mass-transfer resistance might also exist, particularly for a thick film. The internal mass-transfer resistance results from the diffusion of organic molecules within the porous catalyst film. When catalyst is present as a film, the entire catalyst surface is not accessible to the reactant because the reactant must diffuse through the layers of the catalyst. In that case, the relationship among the observed degradation rate, the external and internal mass-transfer rates, and the intrinsic kinetic reaction rate is given by the following expression:

$$\frac{1}{k_o} = \frac{1}{k_r'} + \frac{1}{k_{m,int}\kappa} + \frac{1}{k_{m,ext}\kappa} \quad (8)$$

To determine intrinsic kinetic parameters, it is necessary to find out the mass-transfer rates, so that true kinetic parameters could be deduced from the overall observed rates.

Effect of Internal Mass Transfer. The influence of the internal mass transfer on the observed photocatalytic reaction rate can be determined by the magnitude of the Thiele modulus. The thin catalyst film can be considered a porous slab, and for the first-order reaction, the Thiele modulus (Φ_H) is given by

$$\Phi_H = H\sqrt{\frac{k_r'}{D_e}} \quad (9)$$

where H is the thickness of the catalyst film, k_r' is the first-order kinetic rate constant, and D_e is the effective diffusivity of the pollutant within the catalyst film. Chen and co-workers[28] determined experimentally the effective diffusivity value for benzoic acid as 1×10^{-10} m^2/s. Using the rate constant (k_r) value obtained earlier as 24 μmol/m^3/s, K from the dark reaction as 16.1 m^3/mol, and a film thickness in the range of 2−5 μm, the Thiele modulus value is between 0.0039 and 0.0098, which is ≪1. Therefore, internal mass-transfer resistance could be neglected. In our study, we, therefore, neglected the internal mass-transfer resistance because all of our experiments were conducted at a low catalyst loading of 5.2×10^{-3} kg/m^2. It is worth noting that the internal mass transfer is an intrinsic property of the catalyst film, which depends on the nature of the catalyst, coating techniques, pre- and posttreatment of catalyst films, etc.

Effect of External Mass Transfer. If external mass transfer exists, the reaction rate will depend on the circulation flow rate (Q), particularly when the circulation flow rate is low. External mass-transfer resistance can be reduced to a minimum value by increasing the mixing of the fluid through stirring or increasing the circulation flow rate (Reynolds number) of the reaction medium. To determine whether external mass-transport limitation exists and, if it exists, whether it could be minimized at relatively high circulation flow rates, experiments were performed for photocatalytic degradation of Eosin B at different circulation flow rates. Experimental results for the effect of circulation flow rates on the photocatalytic degradation of Eosin B are shown in Figure 10. The figure confirms significant external mass-transfer limitation when the catalyst is fixed (immobilized) on a surface. It is evident that 5.0×10^{-6} m^3/s is the optimal circulation flow rate for our experimental system where external mass-transfer

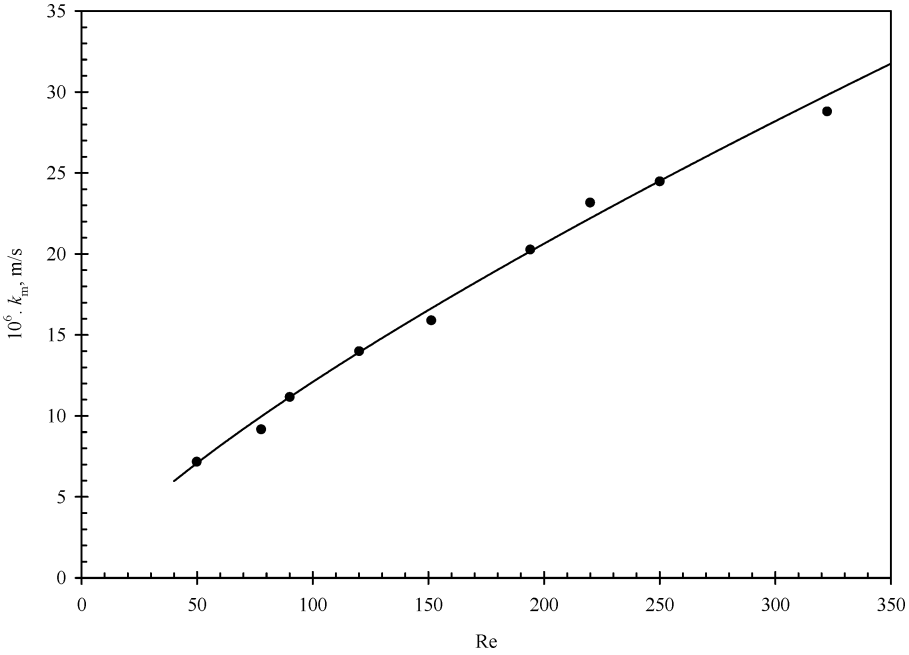

Figure 11. Measurement of the mass-transfer coefficient, k_m, as a function of the Reynolds number. Experimental conditions: $V_L = 2.4 \times 10^{-4}$ m^3, $T = 303$ K, $A = 1.96 \times 10^{-3}$ m^2.

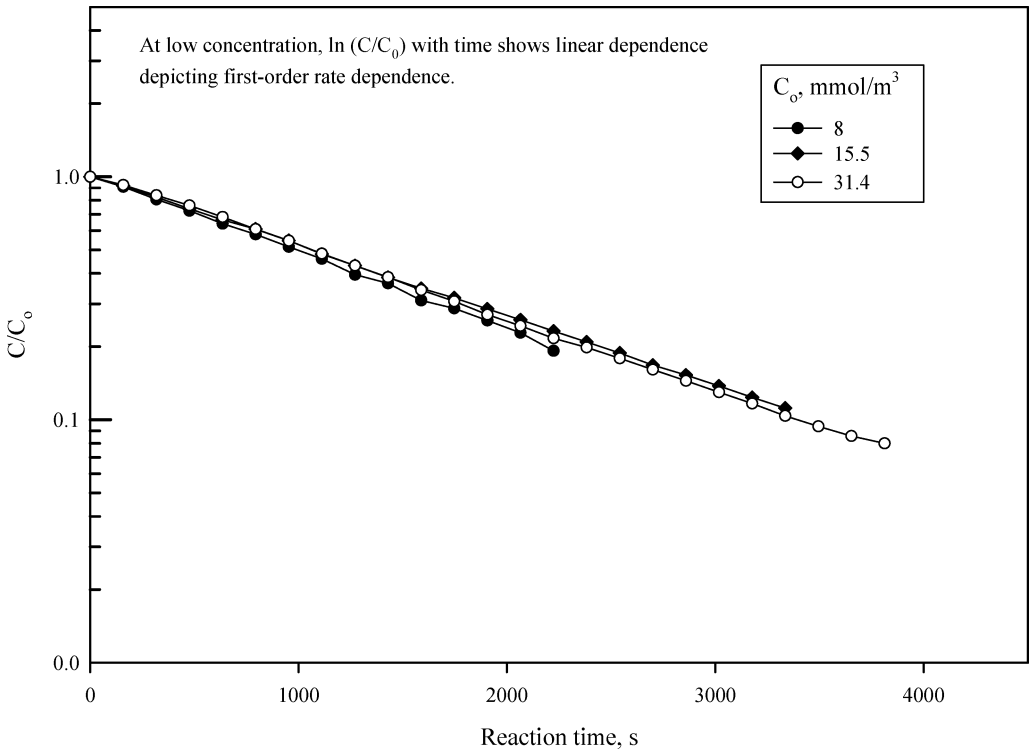

Figure 12. Photocatalytic degradation of Eosin B at low initial concentration. Experimental conditions: SC illumination, $Q = 5.2 \times 10^{-6}$ m^3/s, $I = 33$ W/m^2, $w = 5.2 \times 10^{-3}$ kg/m^2, $V_L = 2.4 \times 10^{-4}$ m^3, $T = 303$ K, $p_{O_2} = 60.8$ kPa, natural pH.

limitation is at a minimum. It should be noted that, at this optimal flow rate, the mass-transfer limitation still exists but is minimal.

Determination of the External Mass-Transfer Rate. External mass transfer depends on the reactor geometry and, therefore, it must be determined with respect to a particular reactor configuration and cannot be used for other reactor systems. In this study, the external mass-transfer coefficient, $k_{m,ext}$, was determined experimentally by measuring the dissolution rate of benzoic acid into water ($C_{out}/C_{sat} \approx 0.04$) at different flow rates at 303 K. The benzoic acid was coated on the inside of the bottom glass plate. The process could be described by the following equation:

$$V_L \frac{dC_b}{dt} = -k_{m,ext} A (C_b - C_s) \qquad (10)$$

where V_L is the total liquid volume (m^3), A is the available surface area of the benzoic acid film (m^2), and C_s and C_b are the concentrations of benzoic acid on the surface of the film and in the bulk solution (mol/m^3), respectively. Because benzoic acid is sparingly soluble in water, C_s was assumed to be equal to the solubility

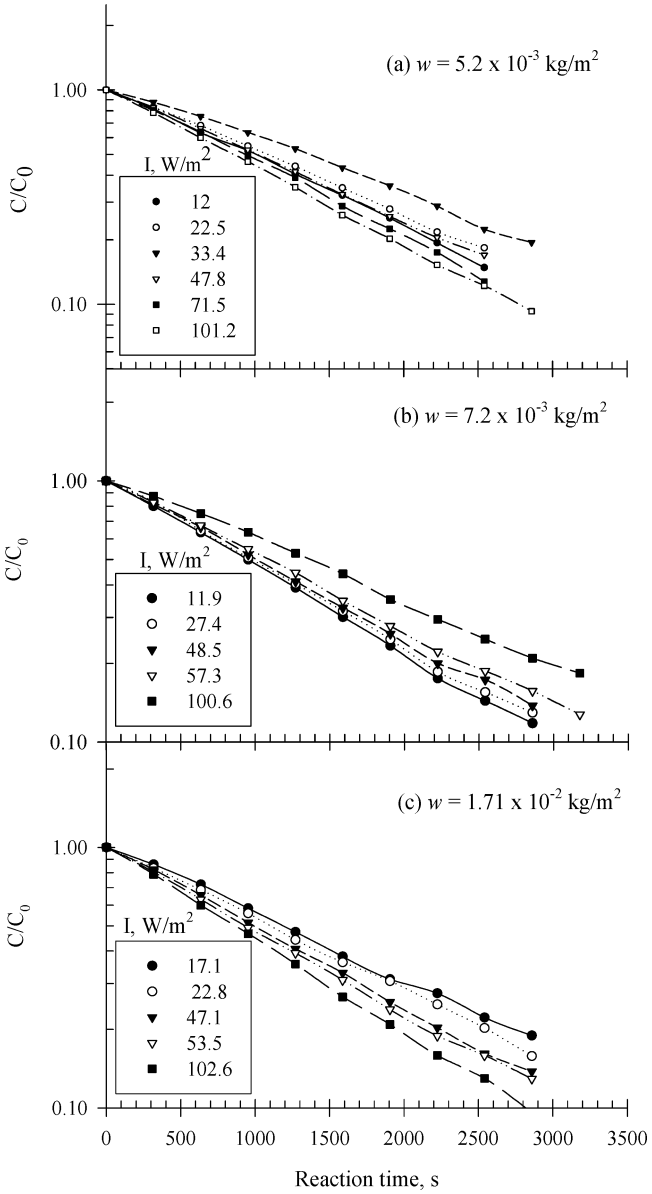

Figure 13. Effect of the light intensity and catalyst layer thickness on the photocatalytic degradation of Eosin B. Experimental conditions: SC illumination, $C_0 = 16$ mmol/m^3, $Re = 141$, $V_L = 2.4 \times 10^{-4}$ m^3, $T = 303$ K, $p_{O_2} = 60.8$ kPa, pH$_0 = 5$, natural pH.

of benzoic acid in water. The experimental results are shown in Figure 11 as a function of the Reynolds number, together with the best fit:

$$k_{m,ext}\,(\text{in m/s}) = 3.49 \times 10^{-7} Re^{0.77} \qquad (11)$$

It is worth noting that at high circulation flow rate external mass-transfer resistance will be a minimum. However, physical limitation on the equipment prevents us from using a very high circulation flow rate because at very high flow rate bubbles will be introduced inside the reactor, which will lead to significant experimental error during measurement. Considering the above fact, all subsequent experiments were performed at a circulation flow rate of 5.0×10^{-6} m^3/s, which is equivalent to a Reynolds number of 141.

The rate constants k_r and K can also be found from a photocatalytic degradation experiment starting with different initial concentrations and then fitting the data with model equation (3) using the k_m value given by eq 11. Figure 12 shows a plot of $\ln[C/C_0]$ with time at a low concentration of Eosin B. From the slope of the lines, we get an average value of k_o (see eq 6) of 2.9×10^{-4} s^{-1} from the three different initial concentrations, respectively. k_r' can now be obtained from eq 8 because $k_{m,ext}$ is known from eq 11. Because k_r was already found to be 24 μmol/m^3/s from experiments at high initial concentration (Figure 9), where the degradation rate followed a zero-order rate (and, therefore, there was no external mass-transfer resistance), the value of K obtained is 14.9 m^3/mol, which is within 8% of the value obtained from the dark reaction experiments (Figure 6), thus suggesting that K indeed represents adsorption characteristics.

Effect of the Light Intensity. It is obvious that the light intensity has a great effect on the photocatalytic reaction rate. In addition, the light may be attenuated as a result of absorption by the catalyst film, when the catalyst is coated on the bottom glass plate (SC illumination). The reaction rate constant usually follows a power-law dependence on light intensities. It has been found for many model compounds that the reaction rate constant is proportional to the square root of the light intensity at high intensity, while at a sufficiently low level of illumination, the reaction rate constant follows first-order dependence.

To investigate the relationship among the reaction rate constant k_r, catalyst loading w (kg/m^2), and light intensity I (W/m^2), experiments were conducted at varying light intensities and catalyst layer thicknesses. The intensity of light falling on the catalyst was varied in our experimental setup by placing different mesh size screens between the lamp and the bottom glass plate. Variation in the catalyst layer thickness was obtained by immobilizing different amounts of catalyst onto the plate by varying the number of dips in dip coating. Figure 13 shows the effect of the intensity of light for three different catalyst layer thicknesses on the photocatalytic degradation of Eosin B. At low concentration ($C_0 = 16$ mmol/m^3), Figure 13 shows that the observed rate follows first-order dependence. In Figure 14, the true rate constants (k_r) are plotted for different values of I and w after correcting for external mass transfer (using k_m as discussed before) from k_o (given by the slope of the lines in Figure 13). The data were fitted with an empirical equation similar to the one reported by Ray and Beenackers[15]

$$k_r = \frac{k_s a w^n I^\beta}{1 + a w^n I^\beta} \qquad (12)$$

By using a nonlinear optimization routine, we found that the above equation fits very well. When the values of k_r, w, and I are expressed respectively as μmol/m^3/s, kg/m^2, and W/m^2, the values obtained for k_s, a, n, and β are 28.3 μmol/m^3/s, 4.3, 0.5, and 0.83, respectively.

Effect of Dissolved Oxygen. In many cases, it has been found that the overall oxidation rate is limited by the removal rate of electrons if a suitable electron scavenger is not present in the system. According to the principles of photocatalytic reaction, the rate of oxidation by holes has to be balanced by the reduction rate of the photogenerated electrons. Accumulated electrons may also result in an increasing rate of the electron−hole recombination step. Hence, an electron scavenger (usually dissolved oxygen) is necessary. Some oxidants,

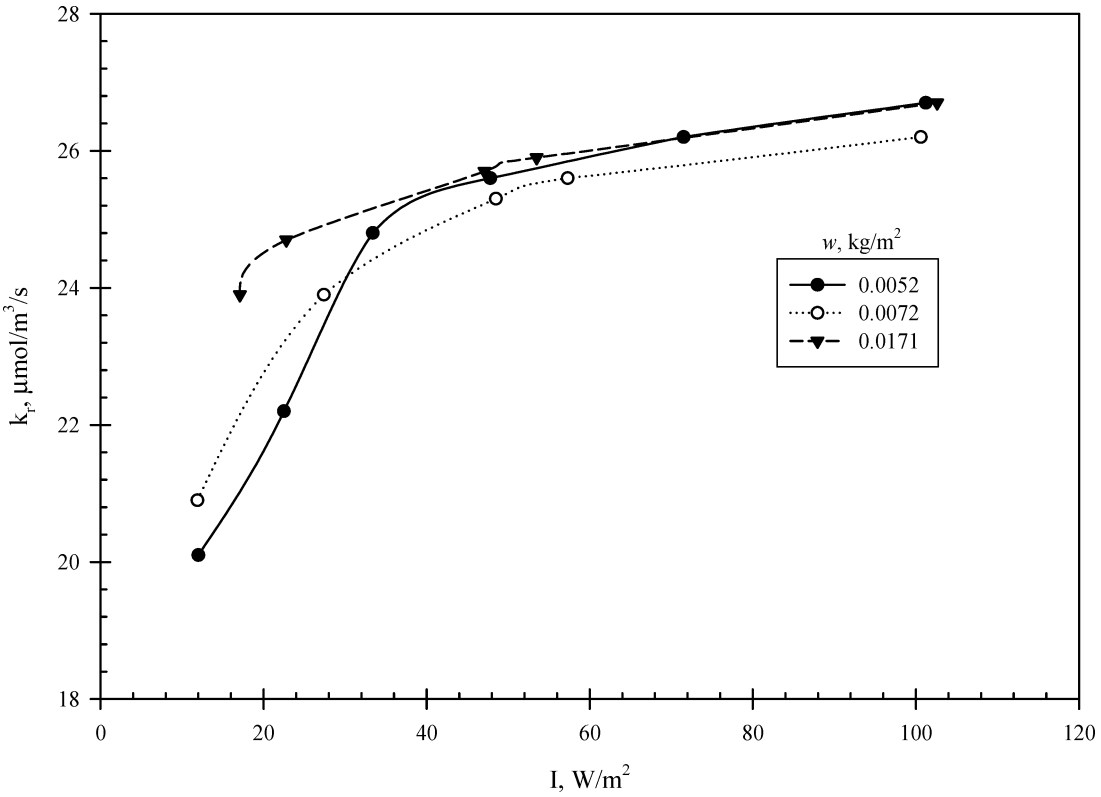

Figure 14. Effect of the light intensity and catalyst layer thickness on the photocatalytic degradation of Eosin B. Experimental conditions: SC illumination, $C_0 = 16$ mmol/m^3, $Re = 141$, $V_L = 2.4 \times 10^{-4}$ m^3, $T = 303$ K, $p_{O_2} = 60.8$ kPa, $pH_0 = 5$, natural pH.

such as O_2, H_2O_2, S_2O_8, Ag^+, etc., have been used as an electron scavenger with some success. However, from a practical point of view, oxygen appears to be the best choice for water treatment. It was found[29] that photocatalytic activity was nearly completely suppressed in the absence of dissolved oxygen and the steady-state concentration of dissolved oxygen had a profound effect on the rate of photocatalyzed decomposition of organic compounds. Alberici and Jardim[30] found that decomposition of phenol in nonaerated solutions containing TiO_2 was much slower compared with that in aerated ones. Sabate et al.[31] did not observe photocatalytic degradation of 3-chlorosalicylic acid when pure N_2 was bubbled through the solution. Hsiao et al.[32] found that the observed rate of disappearance of dichloro- and trichloromethane was much faster when the solution was well purged with oxygen. Gerischer and Heller[33] studied in detail the role of oxygen in the photodestruction of organics on catalyst surfaces. They developed kinetic models to predict the maximum electron uptake by oxygen and found that the latter depends on catalyst particle sizes and the oxygen concentration in the solution.

In our study, this effect was investigated by examining the photocatalytic reaction rates at different partial pressures of dissolved oxygen. The partial pressure of oxygen was adjusted by mixing the oxygen stream with a nitrogen stream, while the total flow rate of the gas was kept at a constant value. The dependence of the observed reaction rate on the partial pressure of oxygen is shown in Figure 15. The figure shows that the observed degradation rate increases with increasing partial pressure of oxygen and reaches a maximum (saturation) value at a partial pressure of oxygen of about 60 kPa. The result also shows that, in commercial application, it is possible to replace pure oxygen with air. In our study, all of the experiments were conducted with saturated oxygen. The dependence of degradation rate constants of organics on the dissolved oxygen concentration can be well described by the Langmuir−Hinshelwood equation:

$$k_p \propto \frac{K_{O_2} p_{O_2}}{1 + K_{O_2} p_{O_2}} \tag{13}$$

When the data were fitted with the above equation, the value of K_{O_2} obtained was 0.478 kPa^{-1}.

Effect of Temperature. The photocatalysis reaction is usually not very temperature-sensitive because the band-gap energy (3.2 eV for TiO_2) is too high to be overcome by thermal activation energy ($kT = 0.026$ eV at room temperature). For example, the overall activation energy for photocatalytic degradation of 4-chlorophenol has been reported as 16 kJ/mol,[1] while for methylene blue, it is 60.6 kJ/mol.[34] Increasing the reaction temperature may increase the oxidation rate of organic compounds at the interface, but it also reduces the adsorptive capacities associated with the organics and dissolved oxygen. Figure 16 shows the effect of temperature on the photocatalytic degradation of Eosin B. Once again, after correction for mass transfer using k_m values, true kinetic rate constants are obtained from the observed rate k_o (given by the slope of the lines in Figure 15). The activation energy was determined from the slope of the Arrhenius plot (see Figure 16) as 25.7 kJ/mol.

Effect of the pH of the Solution. In all of the previous experimental results, the initial pH of the solution was 5, and the subsequent reactions were allowed to continue at natural pH. Some studies have been conducted to investigate the effect of pH on the

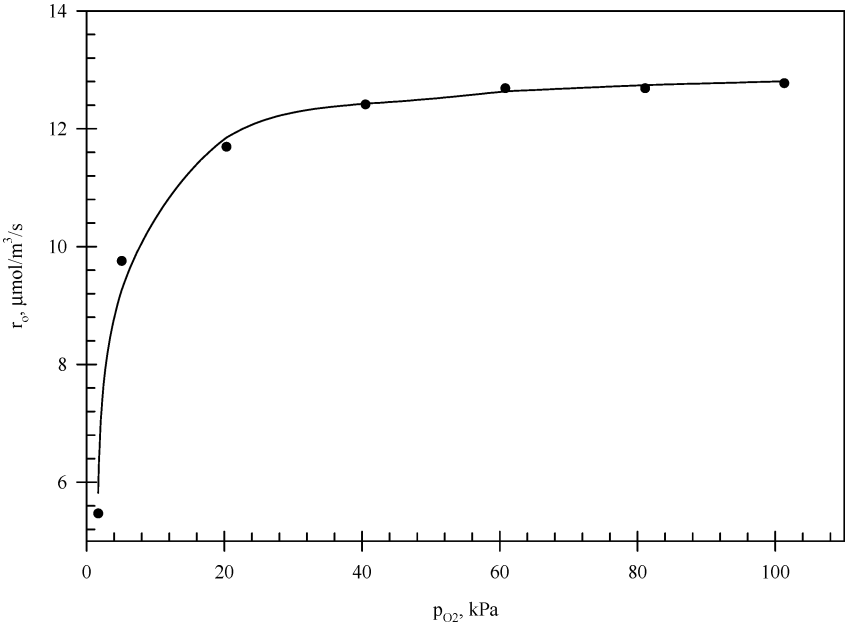

Figure 15. Effect of the partial pressure of oxygen on the photocatalytic degradation of Eosin B. Experimental conditions: SC illumination, $C_0 = 16$ mmol/m^3, $Re = 141$, $V_L = 2.4 \times 10^{-4}$ m^3, $I = 33$ W/m^2, $w = 5.2 \times 10^{-3}$ kg/m^2, $T = 303$ K, $pH_0 = 5$, natural pH.

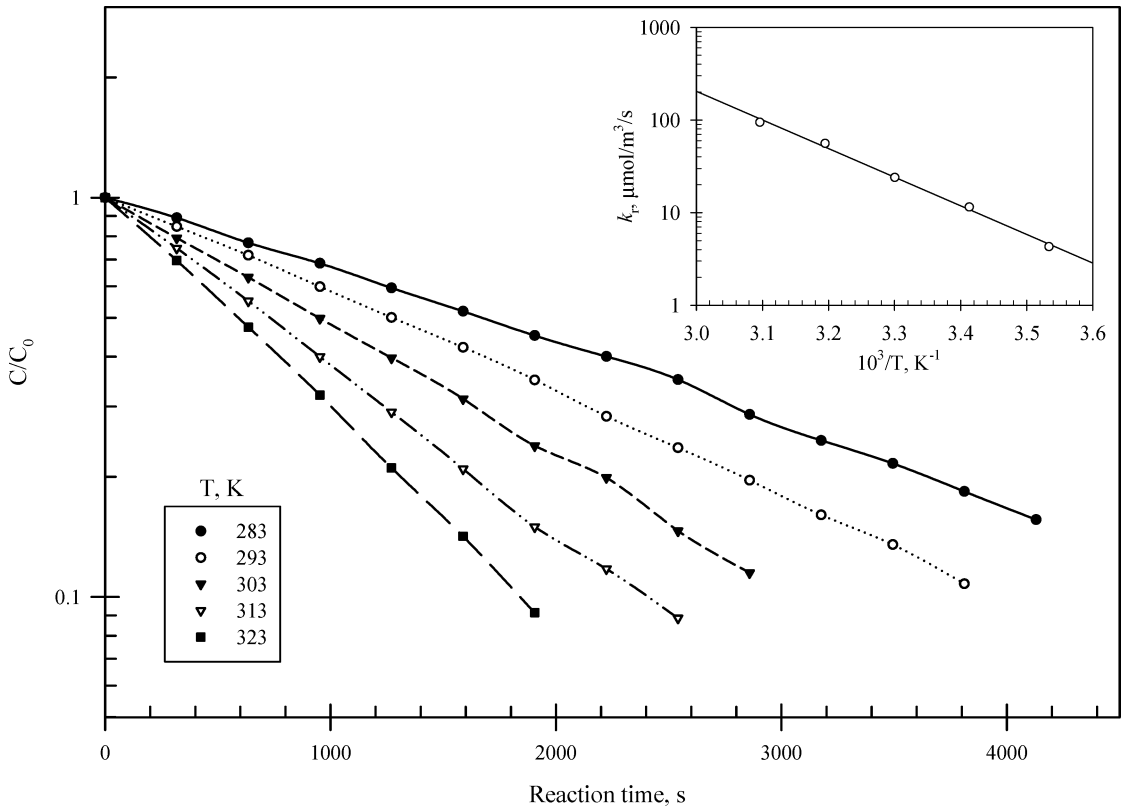

Figure 16. Effect of the temperature on the photocatalytic degradation of Eosin B. Experimental conditions: SC illumination, $C_0 = 16$ mmol/m^3, $Re = 141$, $V_L = 2.4 \times 10^{-4}$ m^3, $I = 33$ W/m^2, $w = 5.2 \times 10^{-3}$ kg/m^2, $p_{O_2} = 60.8$ kPa, $pH_0 = 5$, natural pH.

photocatalytic degradation rate. It is reported that the best pH values for the photocatalytic degradation of some pollutants were near the point of zero charge (pzc). As discussed earlier, the adsorption is mainly attributed to the surface properties of the substrate. The surface charge of Degussa P25 in an aqueous solution as a function of pH is presented in Figure 17. The pH of the point of zero charge was found to be 7.2. For a solution pH greater than 6, the groups with negative charges on the TiO_2 surface are assumed to increase gradually; hence, Eosin B are repelled, and the adsorption of Eosin B is reduced at higher pH values (see Figure 5). Figure 17 shows that a lower pH (acidic condition) can enhance the rate of photocatalytic degradation of Eosin B over a TiO_2 thin film. The effect of pH on the semiconductor band potential and the surface dissociation of the hydrated TiO_2 can explain this behavior. The shift of the band to more negative values with an increase in the pH value leads to a decrease in the oxidation potential of H^+ at high pH. The change in the photo-

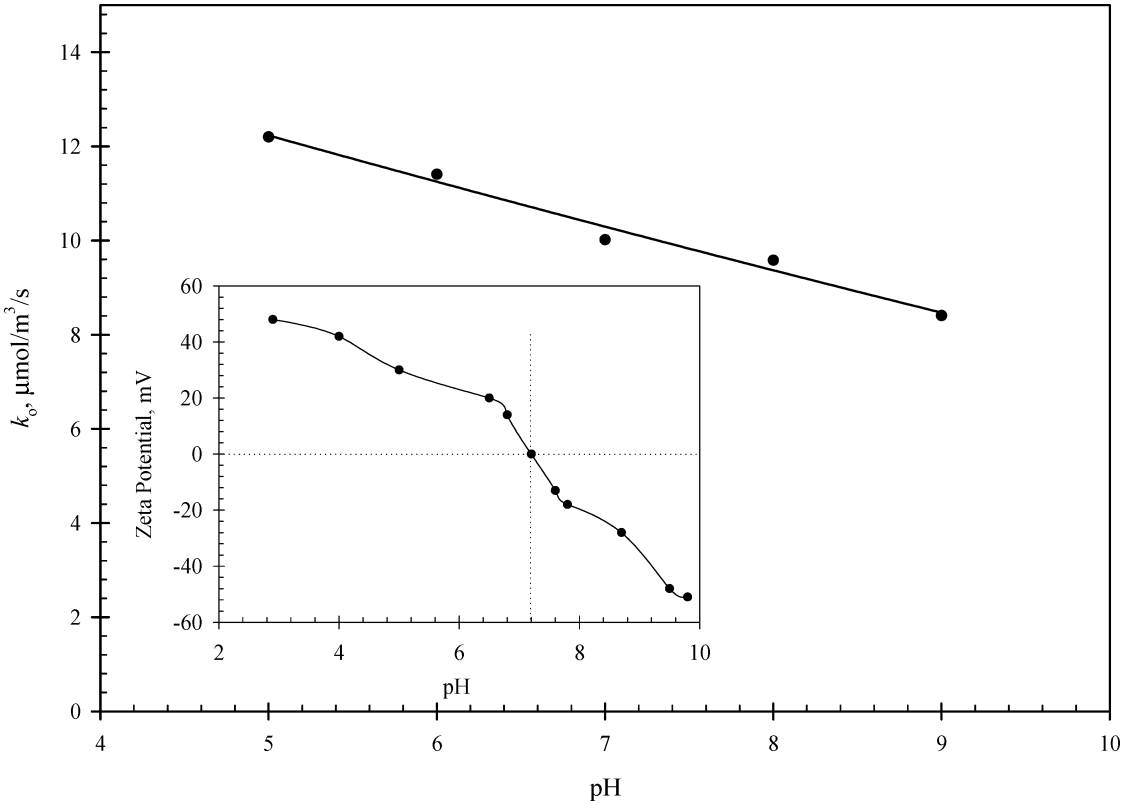

Figure 17. Effect of the pH on the photocatalytic degradation of Eosin B. Experimental conditions: SC illumination, $C_0 = 16$ mmol/m^3, $Re = 141$, $V_L = 2.4 \times 10^{-4}$ m^3, $I = 33$ W/m^2, $w = 5.2 \times 10^{-3}$ kg/m^2, $T = 303$ K, $p_{O_2} = 60.8$ kPa.

catalytic activity at different pH values may be caused by the following dissociation mechanism of TiO_2. It should be noted that TiOH covered the surface of a TiO_2 crystal in the presence of water.

$$\mathrm{TiOH} \leftrightarrow \mathrm{TiO^-} + \mathrm{H^+} \tag{14}$$

In acidic solutions (low pH), the above dissociation will not take place. Thus, the photocatalytic effect is enhanced at a lower pH.

Conclusions

A swirl-flow monolithic-type reactor was used to evaluate the intrinsic kinetic parameters for photocatalytic degradation of a dye, Eosin B when the TiO_2 catalyst was immobilized on the Pyrex glass substrate by a dip-coating technique. The reactor is unique for the kinetic study of photocatalysis because it can be used to measure, apart from various rate constants, the effects of the catalyst layer thickness and light intensity on the rate constants when light falls directly on the catalyst (SC illumination) or when it has to travel through absorbing and scattering liquid media (LC illumination). It was found that external mass-transfer resistance exists and, therefore, true kinetic rates were calculated from the observed reaction rate after correcting for mass resistance. Experiments were also conducted to investigate the effect of temperature, oxygen concentration, and pH. The photocatalytic rates reported with the Degussa P25 catalyst can be described by the following equation:

$$r = k_m \kappa (C_b - C_s) = \frac{k_r(I,w)\, K C_s}{1 + K C_s}$$

where

$$k_m\ (\mathrm{m/s}) = 3.49 \times 10^{-7} Re^{0.77} \qquad \text{for } Re < 250$$

$$k_r(I,w) = \frac{4.3 k_s \sqrt{w} I^{0.83}}{1 + 4.3\sqrt{w} I^{0.83}}$$

$k = 100\ \mathrm{m^{-1}}$, $k_s = 28.3\ \mu\mathrm{mol/m^3/s}$,

$K = 16.1\ \mathrm{m^3/mol}$

$5 < I\ (\mathrm{W/m^2}) < 120$;

$2.0 \times 10^{-3} < w\ (\mathrm{kg/m^2}) < 2.0 \times 10^{-2}$

The reactor appears to be an attractive choice for procuring true kinetic data for different model components and for determining the dependence of various parameters on the photocatalytic degradation rates.

Literature Cited

(1) Mills, A.; Davies, R. H.; Worsley, D. Water Purification by Semiconductor Photocatalysis. *Chem. Soc. Rev.* **1993**, *22*, 417.

(2) Fox, M. A.; Dulay, M. T. Heterogeneous Photocatalysis. *Chem. Rev.* **1993**, *93*, 341.

(3) Legrini, O.; Oliveros, E.; Braun, A. M. Photochemical Processes for Water Treatment. *Chem. Rev.* **1993**, *93*, 671.

(4) Linsebigler, A. L.; Lu, G. Q.; Yates, J. T. Photocatalysis on TiO_2 surfaces—principles, mechanisms, and selected results. *Chem. Rev.* **1995**, *95*, 735.

(5) Hoffmann, M. R.; Martin, S. T.; Choi, W. Y.; Bahnemann, D. W. Environmental applications of semiconductor photocatalysis. *Chem. Rev.* **1995**, *95*, 69.

(6) Mills, A.; LeHunte, S. An overview of semiconductor photocatalysis. *J. Photochem. Photobiol. A* **1997**, *108* (1), 1.

(7) Goswami, D. Y. A review of engineering developments of aqueous phase solar photocatalytic detoxification and disinfection processes. *J. Solar Energy Eng. (Trans. ASME)* **1997**, *119* (2), 101.

(8) Vandevivere, P. C.; Bianchi, R.; Verstraete, W. Treatment and reuse of wastewater from the textile wet-processing industry: Review of emerging technologies. *J. Chem. Technol. Biotechnol.* **1998**, *72* (4), 289.

(9) Herrmann, J. M. Heterogeneous photocatalysis: fundamentals and applications to the removal of various types of aqueous pollutants. *Catal. Today* **1999**, *53*, 115.

(10) Alfano, O. M.; Bahnemann, D.; Cassano, A. E.; Dillert, R.; Goslich, R. Photocatalysis in water environments using artificial and solar light. *Catal. Today* **2000**, *58*, 199.

(11) Chen, D. W.; Sivakumar, M.; Ray, A. K. Semiconductor photocatalysis in environmental remediation. *Dev. Chem. Eng. Miner. Process.* **2000**, *8*, 505.

(12) Bahnemann, D. W. Current challenges in photocatalysis: Improved photocatalysts and appropriate photoreactor engineering. *Res. Chem. Intermed.* **2000**, *26* (2), 207.

(13) Yawalkar, A. A.; Bhatkhande, D. S.; Pangarkar, V. G.; Beenackers, A. A. C. M. Solar-assisted photochemical and photocatalytic degradation of phenol. *J. Chem. Technol. Biotechnol.* **2002**, *77* (1), 102.

(14) Chen, D. W.; Ray, A. K. Removal of toxic metal ions in wastewater by semiconductor photocatalysis. *Chem. Eng. Sci.* **2001**, *56* (4), 1570.

(15) Ray, A. K.; Beenackers, A. A. C. M. Novel swirl-flow reactor for kinetic studies of semiconductor photocatalysis. *AIChE J.* **1997**, *43*, 2571.

(16) Chen, D. W.; Ray, A. K. Photodegradation kinetics of 4-nitrophenol in TiO2 aqueous suspensions. *Water Res.* **1998**, *32*, 3223.

(17) Mukherjee, P. S.; Ray, A. K. Major challenges in the design of a large-scale photocatalytic reactor for water treatment. *Chem. Eng. Technol.* **1999**, *22* (3), 253.

(18) Matthews, R. W. Photooxidation of organic impurities in water using thin films of titanium dioxide. *J. Phys. Chem.* **1987**, *91*, 3328.

(19) Peill, N. J.; Hoffmann, M. R. Chemical and physical characterization of a TiO_2-coated fiber optic cable reactor. *Environ. Sci. Technol.* **1996**, *30*, 2806.

(20) Ray, A. K.; Beenackers, A. A. C. M. Novel photocatalytic reactor for water purification. *AIChE J.* **1998**, *44*, 477.

(21) Ray, A. K.; Beenackers, A. A. C. M. Development of a new photocatalytic reactor for water purification. *Catal. Today* **1998**, *40*, 73.

(22) Ray, A. K. A new photocatalytic reactor for destruction of toxic water pollutants by advanced oxidation process. *Catal. Today* **1998**, *44*, 357.

(23) Ray, A. K. Design, modeling, and experimentation of a new large-scale photocatalytic reactor for water treatment. *Chem. Eng. Sci.* **1999**, *54*, 3113.

(24) Sengupta, T. K.; Kabir, M. F.; Ray, A. K. A Taylor vortex photocatalytic reactor for water purification. *Ind. Eng. Chem. Res.* **2001**, *40*, 5268.

(25) Hepel, M.; Luo, J. Photoelectrochemical mineralization of textile diazo dye pollutants using nanocrystalline WO_3 electrodes. *Electrochim. Acta* **2001**, *47*, 729.

(26) Periyathamby, U.; Ray, A. K. Computer simulation of a novel photocatalytic reactor using distributive computing environment. *Chem. Eng. Technol.* **1999**, *22*, 881.

(27) Chen, D. W.; Ray, A. K. Photocatalytic kinetics of phenol and its derivatives over UV irradiated TiO_2. *Appl. Catal. B* **1999**, *23*, 143.

(28) Chen, D. W.; Li, F. M.; Ray, A. K. Effect of mass transfer and catalyst layer thickness on photocatalytic reaction. *AIChE J.* **2001**, *46*, 1034.

(29) Wang, C. M.; Heller, A.; Gerischer, G. Palladium catalysis of O2 reduction by electrons accumulated on TiO2 particles during photo-assisted oxidation of organic compounds. *J. Am. Chem. Soc.* **1992**, *114*, 5230.

(30) Alberici, R. M.; Jardim, W. F. Photocatalytic degradation of phenol and chlorinated phenols using Ag−TiO_2 in a slurry reactor. *Water Res.* **1994**, *28*, 1845.

(31) Sabate, J.; Anderson, M. A.; Kikkawa, H.; Edwards, M.; Hill, C. G. Kinetic study of the photocatalytic degradation of 3-chlorosalicylic acid over TiO_2 membranes supported on glass. *J. Catal.* **1991**, *127*, 167.

(32) Hsiao, C. Y.; Lee, C. L.; Ollis, D. F. Heterogeneous photocatalysis: Degradation of dilute solutions of CH_2Cl_2, $CHCl_3$, CCl_4 with illuminated TiO_2 photocatalyst. *J. Catal.* **1983**, *82*, 418.

(33) Gerischer, H.; Heller, A. The role of oxygen in photooxidation of organic molecules of semiconductor particles. *J. Phys. Chem.* **1991**, *95*, 5261.

(34) Naskar, S. S.; Pillay, A.; Chanda, M. photocatalytic degradation of organic dyes in aqueous solution with TiO_2 nanoparticles immobilized on foamed polyethylene sheet. *J. Photochem. Photobiol. A* **1998**, *113*, 257.

Received for review April 28, 2003
Revised manuscript received September 5, 2003
Accepted September 17, 2003

IE030366V